Nature. Author manuscript; available in PMC 2014 November 08.

Published in final edited form as:
Nature. 2014 May 8; 509(7499): 245–248. doi:10.1038/nature13310.

Signal amplification and transduction in phytochrome photosensors

Heikki Takala[#1,2], **Alexander Björling**[#2], **Oskar Berntsson**[2], **Heli Lehtivuori**[1], **Stephan Niebling**[2], **Maria Hoernke**[2], **Irina Kosheleva**[4], **Robert Henning**[4], **Andreas Menzel**[3], **Janne A. Ihalainen**[1], and **Sebastian Westenhoff**[2]

[1]Nanoscience Center, Department of Biological and Environmental Science, University of Jyväskylä, 40014 Jyväskylä, Finland [2]Department of Chemistry and Molecular Biology, University of Gothenburg, 40530 Gothenburg, Sweden [3]Paul Scherrer Institut, 5232 Villigen PSI, Switzerland [4]Center for Advanced Radiation Sources, The University of Chicago, IL 60637, USA

[#] These authors contributed equally to this work.

Abstract

Sensory proteins must relay structural signals from the sensory site over large distances to regulatory output domains. Phytochromes are a major family of red-light sensing kinases that control diverse cellular functions in plants, bacteria, and fungi.[1-9] Bacterial phytochromes consist of a photosensory core and a C-terminal regulatory domain.[10,11] Structures of photosensory cores are reported in the resting state[12-18] and conformational responses to light activation have been proposed in the vicinity of the chromophore.[19-23] However, the structure of the signalling state and the mechanism of downstream signal relay through the photosensory core remain elusive. Here, we report crystal and solution structures of the resting and active states of the photosensory core of the bacteriophytochrome from ***Deinococcus radiodurans***. The structures reveal an open and closed form of the dimeric protein for the signalling and resting state, respectively. This nanometre scale rearrangement is controlled by refolding of an evolutionarily conserved “tongue”, which is in contact with the chromophore. The findings reveal an unusual mechanism where atomic scale conformational changes around the chromophore are first amplified into an Ångström

Corresponding author: janne.ihalainen@jyu.fi, westenho@chem.gu.se.

AUTHOR CONTRIBUTIONS

JI, SW, AB, and HT conceived the experiments, HT prepared the samples, crystallized the protein, solved the structure, and measured crystal spectra, AB, HT, SW, JI, SN, HL, MH, AM, RH, and IK performed the solution X-ray scattering experiments, HL performed the spectroscopic measurements in solution, AB performed the MD simulations, AB, HT, OB, and SN analysed data, SW and JI supervised all parts of the project, and SW, JI, HT, and AB wrote the paper with input from all authors.

DATA DEPOSITION:

Coordinates and structure factor amplitudes have been deposited in the RCSB Protein Data Bank, www.pdb.org (PDB ID codes 4O01 and 4OP1). The solution structures are available as source data.

COMPETING FINANCIAL INTEREST

The authors declare no competing financial interest.

SUPPLEMENTARY INFORMATION

Supplementary materials and methods, Source Data, including solution structures, graphical data in ASCII format, full sequence alignment, and force-field parameters for the biliverdin chromophore.

scale distance change in the tongue, and further grow into a nanometre scale conformational signal. The structural mechanism is a blueprint for understanding how the sensor proteins connect to the cellular signalling network.

The most common domain architecture of the photosensory core of phytochromes in bacteria, plants and fungi is PAS-GAF-PHY (Per/Arndt/Sim-cGMP phosphodiesterase/adenyl cyclase/FhlA-phytochromespecific).[10] We investigate the structural dynamics of photoswitching in these domains from the bacteriophytochrome from *D. radiodurans*. Fig. 1a shows that the PAS-GAF-PHY domains share the prototypical response of phytochromes to red/far-red illumination. Its biliverdin chromophore relaxes into the Pr (red-absorbing) state when kept in the dark or after exposure to far-red light. The majority of molecules transform into Pfr (far-red absorbing) state after red light exposure. The dark relaxation from Pfr to Pr occurs in a matter of days, and the optical response of PAS-GAF-PHY is very similar to the full-length protein.[24] For the PHY-less PAS-GAF construct, the absorption spectra (Fig. 1a) and dark reversion within minutes indicate an incomplete photocycle.[24]

Time-resolved solution X-ray scattering reports on structural changes in protein reactions.[25,26] We used it here to characterize the structural dynamics of the phytochrome photocycle. In a first experiment, the phytochrome fragments were repeatedly switched between the Pr and Pfr states using laser flashes of 10 ms duration at 671 nm (Pr $\rightarrow$ Pfr) and 750 nm (Pfr $\rightarrow$ Pr). The X-ray scattering was recorded in between the laser flashes for approximately 1 s and the difference scattering “Pfr” minus “Pr”, $\Delta S(q)$, was calculated (see Supplementary Information for details). These data encode the structural change of the protein during the Pr $\rightarrow$ Pfr transition. For the complete photosensory core (PAS-GAF-PHY) we find a large oscillating difference scattering signal at low angles $q < 2$ nm^{-1} (Fig. 1b, red line), indicating large structural changes on the nanometre scale. Oscillations at higher q, which report on structural changes on smaller length scales, were also observed (Extended Data Figure 1e), but are not discussed further here. The laser-induced ΔS of the PAS-GAF-PHY construct was reproduced by a standard Small-Angle X-ray Scattering (SAXS) experiment with pre-illuminated samples (Fig. 1b, blue line). Time-resolved difference X-ray scattering data covering the micro- and millisecond time scales also reproduce these features when photoconversion is complete (delay time: 30 ms, Fig. 1b, black line). These data further establish that the discussed low-q features grow in with a time-constant of 4.3 ms (Fig. 1b, Extended Data Figure 1d), which coincides with the formation of the Pfr state as measured by optical absorption of the chromophore (1.0 ms, Extended Data Figure 1d).

When performing the same experiments on the PHY-less photosensory core (PAS-GAF), the oscillatory signal at low-q is absent (Fig. 1c). The observed oscillations in the PAS-GAF domains are much smaller in amplitude and confined to higher q ranges (Fig. 1c and Extended Data Figure 1e). These data show that quaternary structural changes occur only when the PHY domain is present. In the wild-type protein the PHY domain connects the chromophore binding domains PAS/GAF with the output kinase, making it likely that the detected rearrangement is functionally relevant.

Europe PMC Funders Author Manuscripts

In order to examine the nature of these conformational changes and to find out how they arise, we crystallised the photosensory core in the dark (referred to as *dark*) and under periodic illumination at 655 nm (referred to as *illuminated*), which transforms a large fraction of the protein molecules into the Pfr state (Fig. 1a and Extended Data for details). Absorption spectra of the *dark* crystals indicate the Pr state, while the *illuminated* crystals are Pfr-enriched (Extended Data Figure 3c). Omit maps indicate a change in the conformation of the chromophore between the two crystal forms (Extended Data Figure 3b). Although the biliverdin conformation cannot be fit unambiguously to the electron density in the *illuminated* structure, the electron density of the rest of the protein is homogeneous (Extended Data Figure 2b).

Our dark crystal structure was modelled from data up to 3.80 Å resolution (Fig. 2a). The observed domain arrangement is similar to previously reported structures of bacterial PAS-GAF and PAS-GAF-PHY protein fragments,[12-15,17] but the dimer arrangement differs to some of these structures.[13,17] The *illuminated* structure, modelled against data cut at 3.24 Å, shows dramatic differences compared to the *dark* structure (Fig. 2a). Firstly, the dimer adopts an open Y-like shape of the PHY domains. This is in contrast to all reported resting state structures, where the dimer is closed (Fig. 2a).[12,13,17,20] Secondly, the tongue of the PHY domains (residues 446-477) appears as an α-helix and a loop in the *illuminated* model and is a β-sheet in the *dark* model (Fig. 2b and Extended Data Figure 2). These two folds have been observed separately in prototypical cyanobacterial[13,17] and non-canonical bacterial phytochromes,[12,20] respectively (Extended Data Figure 4). Our structures establish that the refolding of the tongue occurs within the same bacterial phytochrome, and suggest that this refolding is associated with opening of the dimer. The change in fold causes the length of the tongue to vary between the *dark* and *illuminated* structures (Fig. 2b), which is key for understanding the role of the tongue in signal relay.

Before detailing this mechanism, it is important to test how well the crystal models represent the solution structures of the Pr and Pfr states. To this end, we performed structural refinement against the solution *difference* X-ray scattering data (Fig. 1), which is a sensitive indicator of conformational change. It has the advantage over *absolute* scattering profiles that experimental error and uncertainties arising from the choice of method for scattering calculations largely cancel out (Extended Data 5.

We generated candidate solution structures by running two sets of molecular dynamics (MD) simulations starting from the *dark* and *illuminated* crystal structures (see Supplementary Information for details). These are referred to as Pr and Pfr trajectories since they aim to model solution scattering data representing these states. Snapshots were recorded every 50 ps and the solution X-ray scattering was calculated from each. All pairs of Pr/Pfr candidate structures were then compared to the static difference X-ray scattering (Fig. 1b, Extended Data Fig. 7, see Supplementary Information for details). We selected the 100 Pr/Pfr pairs with best agreement to the data and consider the participating structures to be representative of the protein in solution. Considering all pairwise differences between these structures, a consistent set of 747 curves was generated and evaluated (Fig. 3a). The agreement of the model and experiment is excellent, and striking improvement is made compared to the crystal structures.

In order to verify the choice of solution structures based on difference scattering, these structures were cross-validated against absolute, population-corrected SAXS data as described in Supplementary Information (see also Extended Data Figure 5). Fig. 3b shows that the agreement with absolute SAXS data is strongly correlated with the separation of the PHY domains, and that the solution structures, proposed purely on difference scattering, cluster in the low-error parts of these correlations. The agreement of the solution structures to the solution scattering is significantly improved compared to the crystal structures as can be seen in Fig. 3b. Representative structural models for Pr and Pfr states in solution are depicted in Fig. 4.

The solution-structural models show that the PHY domains of opposing monomers come fairly close to each other in the Pr state but move apart by ~3 nm during the Pr → Pfr transition (Fig. 4). The Y shape assumed by the solution structures in the Pfr state is in qualitative agreement with a low-resolution envelope of a *Rps. Palustris* phytochrome determined by SAXS.[27] Our crystal structures capture the essence of this quaternary conformational change, albeit with differences in the amplitude and details of the motion. These differences are likely caused by crystal contacts (Extended Data Figure 6). Nevertheless, the overall agreement with the solution structures lends strong support to that the refolding of the tongue observed in the crystal structures is intrinsic to the structural rearrangement between Pr and Pfr states. From the crystal and solution structures the following mechanism for signal transduction through the photosensory core emerges. It is known that the rotation of the biliverdin D-ring causes atomic rearrangements in the chromophore binding pocket, including displacement of Asp207 and Tyr263.[19-22] Our crystal structures suggest that this controls the fold of the tongue of the PHY domain. Importantly, the tongue is shortened as a result of the refolding and the distance between the GAF and PHY domain is reduced by 2.5 Å (Fig. 2b) upon red-light illumination. As a consequence of this, and demonstrated by our Pr and Pfr solution structures, the dimer opens up between the PHY domains by several nanometres (Fig. 4).

Three factors are essential for the proposed structural mechanism. Firstly, the PHY and GAF/PAS domains, which are connected by the tongue, are known to be very rigid internally such that they cannot deform to absorb the length variation of the tongue.[11] Secondly, the tongue and its junctions to PHY and GAF have to be rigid, especially in Pr where the PHY and GAF domains are pushed away from each other. In our *dark* structures the direction of the tongue is rigidly fixed with respect to the GAF domains by the conserved interaction Arg466 to Asp207/Tyr263 and additional backbone hydrogen bonding (Fig. 2b).[13] In the *illuminated* structure the tongue binds to GAF through interaction of Ser468 with Asp207/Tyr263,[12] and through hydrophobic interactions, among others by Tyr472 (Extended Data Fig. 4b).[17] The tongue is also locked close to the PHY domain by additional backbone hydrogen bonding. Thirdly, the PAS/GAF and PHY domains are connected by the unusually long scaffolding helix, which is necessary to redirect the shortening of the tongue into bending of the monomer. Indeed, our simulations reveal a hinge in the scaffolding helix (Fig. 4b). All phytochrome structures published to date support these three requirements.[12-18]

In bacterial and fungal phytochromes signal output is through C-terminal histidine kinase domains which autophosphorylate and further phosphotransfer to a response regulator.[3,7] In plant phytochromes two additional PAS domains are included in the C-terminal regulatory region and a more complex pattern of functions has to be controlled, such as serine/threonine kinase activity,[4] and affinity to interaction partners.[9,10] In all cases, the output activity is likely controlled by a structural change in the photosensory core. The photosensory core and the key amino acid sequence in the tongue region ^{465}PRxSF^{469} are highly conserved over the whole phytochrome superfamily (Extended Data Figure 2c). We suggest here a mechanism, in which the fold of the PHY-tongue controls the bending of the monomer. For the isolated photosensory unit in this study, this results in dramatic opening of the dimer in Pfr (Fig. 2 and Fig. 4). In full-length phytochromes it becomes conceivable that distances between output domains is modified. Alternatively, previously buried patches of the protein could become accessible to interaction partners, or monomers could rearrange with respect to each other. It will be intriguing to see the emergence of these mechanisms, which become deductible with experimental approaches similar to the one presented here.

METHODS SUMMARY

The PAS-GAF-PHY and PAS-GAF fragments from *Deinococcus radiodurans* were expressed in the *Escherichia coli* strain BL21 (DE3) and purified by affinity and size-exclusion chromatography. Crystallographic data was collected at beamline ID23-1 of the ESRF (see Extended Data Table 1). Time-resolved X-ray scattering with millisecond time resolution were recorded at beamline cSAXS of the Swiss Light Source.[28] SAXS measurements were performed at beamline BM29 of the European Synchrotron Radiation Facility (ESRF) and analysed as summarised in Extended Data Table 2a. Time-resolved X-ray scattering data in the micro- and millisecond ranges were collected at beamline ID-14-B, BioCARS, of the Advanced Photon Source at Argonne National Laboratory. All solution scattering sample details are summarized in Extended Data Table 2b. Molecular dynamics simulations (GROMACS 4.5.5)[29] were used to generate trial solution structures and theoretical scattering curves were evaluated using Zernike expansion as implemented in SASTBX.[30] The structures were scored against experimental scattering data as detailed in Supplementary Information.

Supplementary Material

Refer to Web version on PubMed Central for supplementary material.

ACKNOWLEDGEMENTS

We acknowledge beamline access at BM29 and ID23-1 at the ESRF, cSAXS at the Swiss Light Source, funding for which was received from the European Community's FP7 grant agreement n.°312284 (CALIPSO), and BioCARS (supported by National Institutes of Health, National Institute of General Medical Sciences grant 1R24GM111072 and in part through collaboration with Philip Anfinrud) at the Advanced Photon Source, Argonne National Laboratory. K. Forest and R. Vierstra are acknowledged for the donation of the plasmids. Jari Ylänne and his group are acknowledged for advice on crystallography, and Heikki Häkkänen and Alli Liukkonen for their assistance. We thank Maria-Andrea Mroginski for kindly providing force-field parameter files for the biliverdin. We acknowledge Vladimir Chukharev and Nikolai V. Tkachenko at the Department of Chemistry and Bioengineering, Tampere University of Technology for the facilities for transient absorption spectroscopy measurements. We also acknowledge grants to SW by the Foundation of Strategic Research, Sweden, and the Swedish and European

Research Councils, support to JI by Finnish Academy grant 138063, and to HT by the Finnish Cultural Foundation grant 0131067.

REFERENCES

1. Butler WL, Norris KH, Siegelman HW, Hendricks SB. Detection, Assay, and Preliminary Purification of the Pigment Controlling Photoresponsive Development of Plants. Proc. Natl. Acad. Sci. U. S. A. 1959; 45:1703–1708. doi:DOI 10.1073/pnas.45.12.1703. [PubMed: 16590561]
2. Kehoe DM, Grossman AR. Similarity of a chromatic adaptation sensor to phytochrome and ethylene receptors. Science. 1996; 273:1409–1412. doi:DOI 10.1126/science.273.5280.1409. [PubMed: 8703080]
3. Yeh KC, Wu SH, Murphy JT, Lagarias JC. A cyanobacterial phytochrome two-component light sensory system. Science. 1997; 277:1505–1508. doi:DOI 10.1126/science.277.5331.1505. [PubMed: 9278513]
4. Yeh K-C, Lagarias JC. Eukaryotic phytochromes: Light-regulated serine/threonine protein kinases with histidine kinase ancestry. Proceedings of the National Academy of Sciences. 1998; 95:13976–13981. doi:10.1073/pnas.95.23.13976.
5. Jiang ZY, et al. Bacterial photoreceptor with similarity to photoactive yellow protein and plant phytochromes. Science. 1999; 285:406–409. doi:DOI 10.1126/science.285.5426.406. [PubMed: 10411503]
6. Hughes J, et al. A prokaryotic phytochrome. Nature. 1997; 386:663–663. doi:Doi 10.1038/386663a0. [PubMed: 9109482]
7. Bhoo SH, Davis SJ, Walker J, Karniol B, Vierstra RD. Bacteriophytochromes are photochromic histidine kinases using a biliverdin chromophore. Nature. 2001; 414:776–779. doi:Doi 10.1038/414776a. [PubMed: 11742406]
8. Blumenstein A, et al. The Aspergillus nidulans phytochrome FphA represses sexual development in red light. Curr Biol. 2005; 15:1833–1838. doi:DOI 10.1016/j.cub.2005.08.061. [PubMed: 16243030]
9. Ni M, Tepperman JM, Quail PH. Binding of phytochrome B to its nuclear signalling partner PIF3 is reversibly induced by light. Nature. 1999; 400:781–784. [PubMed: 10466729]
10. Rockwell NC, Su YS, Lagarias JC. Phytochrome structure and signaling mechanisms. Annual Review of Plant Biology. 2006; 57:837–858. doi:DOI 10.1146/annurev.arplant.56.032604.144208.
11. Moglich A, Yang XJ, Ayers RA, Moffat K. Structure and Function of Plant Photoreceptors. Annu Rev Plant Biol. 2010; 61:21–47. doi:DOI 10.1146/annurev-arplant-042809-112259. [PubMed: 20192744]
12. Yang X, Kuk J, Moffat K. Crystal structure of Pseudomonas aeruginosa bacteriophytochrome: Photoconversion and signal transduction. Proc. Natl. Acad. Sci. U. S. A. 2008; 105:14715–14720. doi:DOI 10.1073/pnas.0806718105. [PubMed: 18799746]
13. Essen LO, Mailliet J, Hughes J. The structure of a complete phytochrome sensory module in the Pr ground state. Proc. Natl. Acad. Sci. U. S. A. 2008; 105:14709–14714. doi:DOI 10.1073/pnas.0806477105. [PubMed: 18799745]
14. Wagner JR, Brunzelle JS, Forest KT, Vierstra RD. A light-sensing knot revealed by the structure of the chromophore-binding domain of phytochrome. Nature. 2005; 438:325–331. doi:Doi 10.1038/Nature04118. [PubMed: 16292304]
15. Li H, Zhang JR, Vierstra RD, Li HL. Quaternary organization of a phytochrome dimer as revealed by cryoelectron microscopy. Proc. Natl. Acad. Sci. U. S. A. 2010; 107:10872–10877. doi:DOI 10.1073/pnas.1001908107. [PubMed: 20534495]
16. Cornilescu G, Ulijasz AT, Cornilescu CC, Markley JL, Vierstra RD. Solution Structure of a Cyanobacterial Phytochrome GAF Domain in the Red-Light-Absorbing Ground State. J. Mol. Biol. 2008; 383:403–413. doi:DOI 10.1016/j.jmb.2008.08.034. [PubMed: 18762196]
17. Anders K, Daminelli-Widany G, Mroginski MA, von Stetten D, Essen LO. Structure of the Cyanobacterial Phytochrome 2 Photosensor Implies a Tryptophan Switch for Phytochrome Signaling. Journal of Biological Chemistry. 2013; 288:35714–35725. doi:DOI 10.1074/jbc.M113.510461. [PubMed: 24174528]

Europe PMC Funders Author Manuscripts

18. Narikawa R, et al. Structures of cyanobacteriochromes from phototaxis regulators AnPixJ and TePixJ reveal general and specific photoconversion mechanism. Proc. Natl. Acad. Sci. U. S. A. 2013; 110:918–923. doi:DOI 10.1073/pnas.1212098110. [PubMed: 23256156]
19. Yang XJ, Kuk J, Moffat K. Conformational differences between the Pfr and Pr states in Pseudomonas aeruginosa bacteriophytochrome. Proc. Natl. Acad. Sci. U. S. A. 2009; 106:15639–15644. doi:DOI 10.1073/pnas.0902178106. [PubMed: 19720999]
20. Yang XJ, Ren Z, Kuk J, Moffat K. Temperature-scan cryocrystallography reveals reaction intermediates in bacteriophytochrome. Nature. 2011; 479:428–U190. doi:Doi 10.1038/Nature10506. [PubMed: 22002602]
21. Song C, et al. Two ground state isoforms and a chromophore D-ring photoflip triggering extensive intramolecular changes in a canonical phytochrome. Proc. Natl. Acad. Sci. U. S. A. 2011; 108:3842–3847. doi:DOI 10.1073/pnas.1013377108. [PubMed: 21325055]
22. Burgie ES, Walker JM, Phillips GN, Vierstra RD. A Photo-Labile Thioether Linkage to Phycoviolobilin Provides the Foundation for the Blue/Green Photocycles in DXCF-Cyanobacteriochromes. Structure. 2013; 21:88–97. doi:DOI 10.1016/j.str.2012.11.001. [PubMed: 23219880]
23. Ulijasz AT, et al. Structural basis for the photoconversion of a phytochrome to the activated Pfr form. Nature. 2010; 463:250–U143. doi:Doi 10.1038/Nature08671. [PubMed: 20075921]
24. Wagner JR, et al. Mutational analysis of Deinococcus radiodurans bacteriophytochrome reveals key amino acids necessary for the photochromicity and proton exchange cycle of phytochromes. Journal of Biological Chemistry. 2008; 283:12212–12226. doi:DOI 10.1074/jbc.M709355200. [PubMed: 18192276]
25. Cammarata M, et al. Tracking the structural dynamics of proteins in solution using time-resolved wide-angle X-ray scattering. Nature Methods. 2008; 5:881–886. doi:10.1038/nmeth.1255. [PubMed: 18806790]
26. Andersson M, et al. Structural Dynamics of Light-Driven Proton Pumps. Structure. 2009; 17:1265–1275. doi:10.1016/j.str.2009.07.007. [PubMed: 19748347]
27. Evans K, Grossmann JG, Fordham-Skelton AP, Papiz MZ. Small-angle x-ray scattering reveals the solution structure of a bacteriophytochrome in the catalytically active Pr state. J. Mol. Biol. 2006; 364:655–666. doi:DOI 10.1016/j.jmb.2006.09.045. [PubMed: 17027028]
28. Westenhoff S, et al. Rapid readout detector captures protein time-resolved WAXS. Nature Methods. 2010; 7:775–776. [PubMed: 20885435]
29. Pronk S, et al. GROMACS 4.5: a high-throughput and highly parallel open source molecular simulation toolkit. Bioinformatics. 2013; 29:845–854. [PubMed: 23407358]
30. Liu HG, Hexemer A, Zwart PH. The Small Angle Scattering ToolBox (SASTBX): an open-source software for biomolecular small-angle scattering. J Appl Crystallogr. 2012; 45:587–593. doi:Doi 10.1107/S0021889812015786. 10.1074/jbc.M611824200 (2007).

Extended Data References

31. Sievers F, et al. Fast, scalable generation of high-quality protein multiple sequence alignments using Clustal Omega. Mol Syst Biol. 2011; 7 doi:http://www.nature.com/msb/journal/v7/n1/suppinfo/msb201175_S1.html.
32. Wagner JR, Zhang JR, Brunzelle JS, Vierstra RD, Forest KT. High resolution structure of Deinococcus bacteriophytochrome yields new insights into phytochrome architecture and evolution. Journal of Biological Chemistry. 2007; 282:12298–12309. doi:DOI 10.1074/jbc.M611824200. [PubMed: 17322301]
33. Mailliet J, et al. Spectroscopy and a High-Resolution Crystal Structure of Tyr263 Mutants of Cyanobacterial Phytochrome Cph1. J. Mol. Biol. 2011; 413:115–127. doi:DOI 10.1016/j.jmb.2011.08.023. [PubMed: 21888915]
34. Konarev PV, Volkov VV, Sokolova AV, Koch MHJ, Svergun DI. PRIMUS: a Windows PC-based system for small-angle scattering data analysis. J Appl Crystallogr. 2003; 36:1277–1282. doi:Doi 10.1107/S0021889803012779.

35. Anders K, Daminelli-Widany, Mroginski MA, Von Stetten D, Essen LO. Structure of the cyanobacterial phytochrome 2 photosensor implies a tryptophan switch for phytochrome signaling. The Journal of Biological Chemistry. 2013 published online, doi:10.1074/jbc.M113.510461.

36. Gasteiger, E., et al. The Proteomics Protocols Handbook. Walker, JohnM, editor. Humana Press; 2005. p. 571-607.Ch. 52

Europe PMC Funders Author Manuscripts

Europe PMC Funders Author Manuscripts

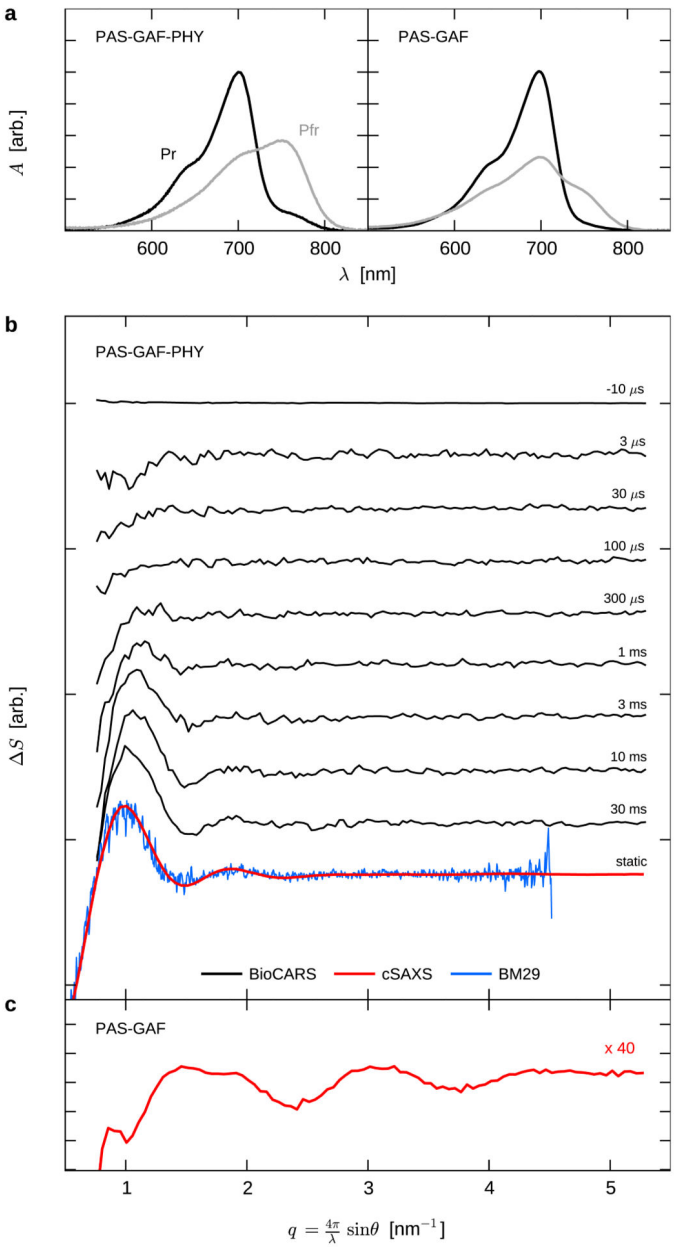

Figure 1. Time-resolved solution X-ray scattering of the PAS-GAF and PAS-GAF-PHY fragments from *D. radiodurans*

a, Absorption spectra of protein fragments after illumination with far-red (780 nm) and red (655 nm) light, labelled Pr and Pfr respectively. **b** and **c**, Solution X-ray scattering data from the PAS-GAF-PHY and PAS-GAF fragments shown on the same scale. Time-resolved data (black, BioCARS), direct static data collected by laser-induced population switching (red, cSAXS), and indirect static data from a standard SAXS experiment with pre-illuminated samples (blue, BM29) is shown. Δ*S* is the difference in scattered X-ray intensity caused by illumination at 671 nm. $q = 4\pi/\lambda \cdot \sin\theta$ at wavelength λ and scattering angle 2θ.

Europe PMC Funders Author Manuscripts

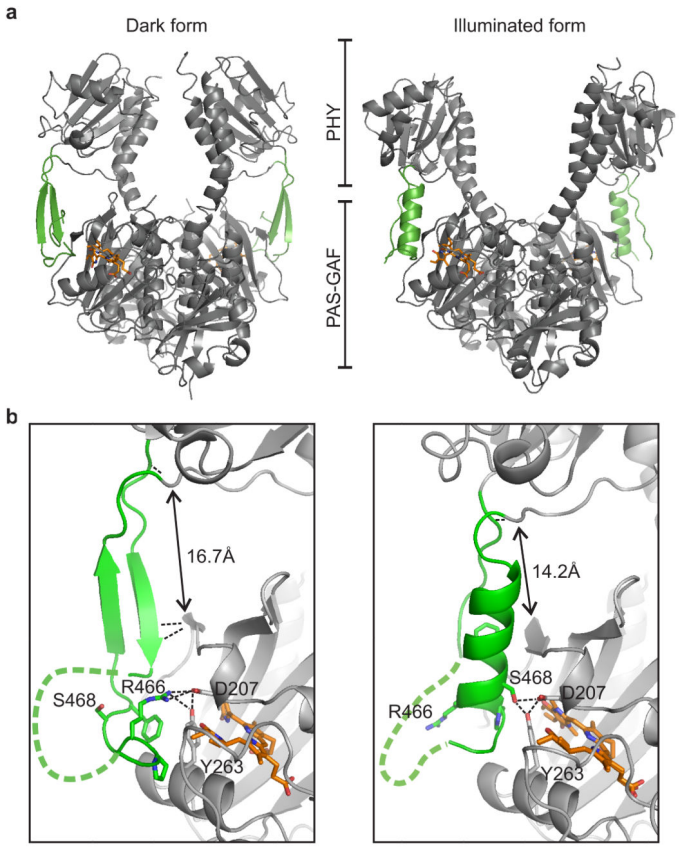

Figure 2. Dark and illuminated crystal structures of PAS-GAF-PHY from *D. radiodurans*

a, Crystal structures of the PAS-GAF-PHY dimer in the *dark* and *illuminated* forms. The tongue of the PHY domain (green) changes fold and the dimer opens up in the illuminated state. The biliverdin chromophore is shown in orange. **b**, Fold and interactions of the PHY tongue. The β-sheet (*dark*) coordinates to Asp207 and Tyr263 via Arg466, whereas the α-helix (*illuminated*) coordinates via Ser468, both of which are part of the conserved ^{465}PRxSF^{469} motif. The named residues are shown as sticks. The β-sheet (*dark*) is further held by hydrogen bonding interactions between the amide groups of Ala450, Gly452 and Arg202. The change in PHY domain conformation leads to a shortening of the tongue by 2.5 Å as measured between GAF (Arg202) and PHY (Tyr479) domains (arrows). A backbone interaction close to the PHY domain between Leu445 and Tyr479, shared by both crystal structures, is also indicated. The green dashed lines indicate regions that are not modelled or not shown for clarity.

Europe PMC Funders Author Manuscripts

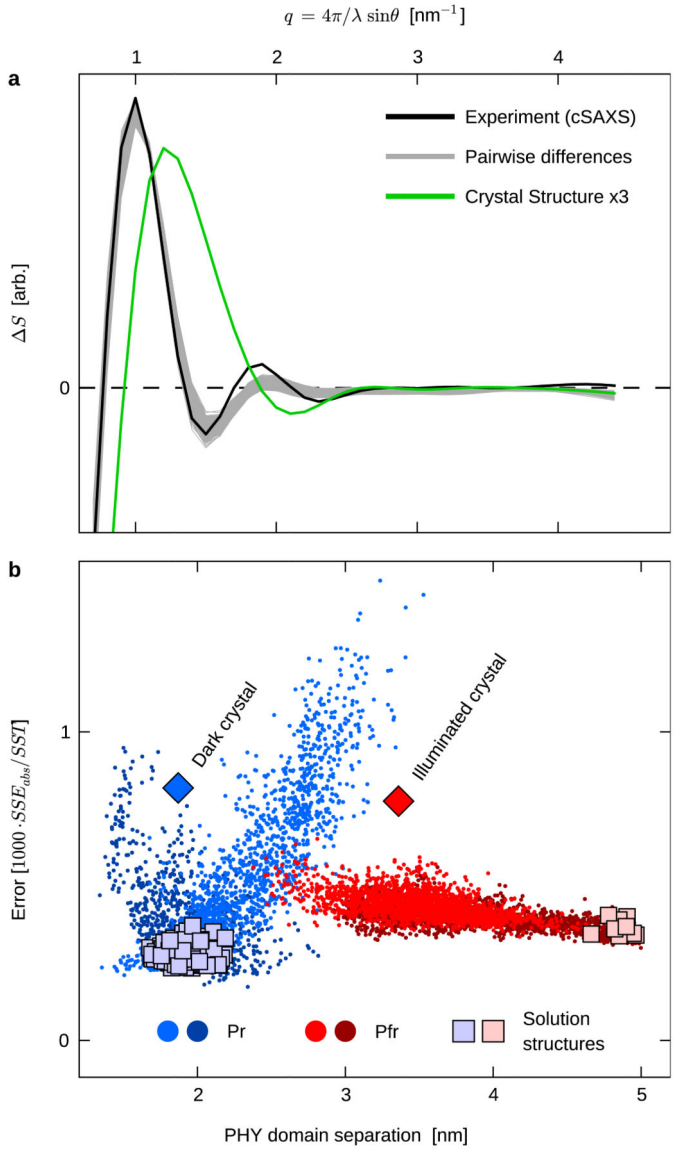

Figure 3. Refinement of solution structures against difference SAXS data

a, Calculated differences X-ray scattering between the proposed solution structures (Pfr-Pr, grey) agree with experimental data (black). As a safeguard against overfitting, the grey curves show all 747 differences between solution structures, not just the 100 best curves on which the pairs were selected (See text for details). The agreement with experiment is dramatically improved for the solution structures, compared to the difference scattering calculated from the two crystal forms (green). **b**, Validation of the obtained solution structures (squares) against absolute X-ray scattering. All MD snapshots (dots) and crystal structures (diamonds) are scored against absolute SAXS data (BM29) after correction for the mixed Pr/Pfr populations (see Extended Data Figure 5d). The two shades of red and blue correspond to different simulation conditions as detailed in Supplementary Information. The PHY domain separation is measured as the distance between the centers of mass of the two C-terminal helices (residues 484-503).

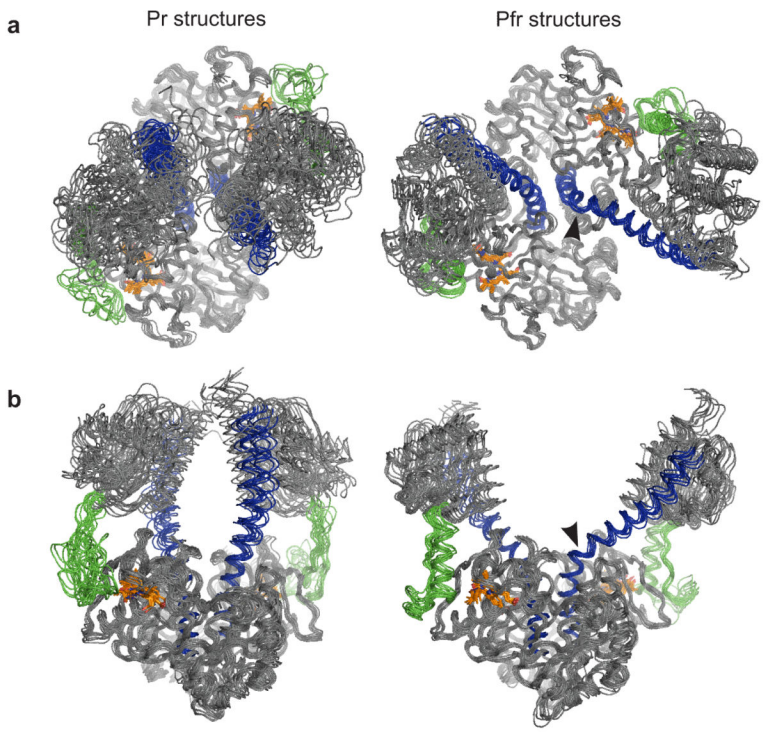

Figure 4. Proposed solution structures of the bacterial phytochrome from *D. radiodurans*

Representative solution structures for the Pr and Pfr states of the photosensory core, identified from solution X-ray scattering experiments. Nine Pfr and ten Pr structures are presented viewed along (**a**) and perpendicular (**b**) to the dimer symmetry axis. The long scaffolding helix is highlighted in blue, the PHY tongue in green, and the biliverdin chromophore in orange. The PHY domain separation differs by about 3 nm between the Pr and Pfr structures as shown in Figure 3b. The hinge region at the scaffolding helix (residues Val318 and Lys319) in Pfr is indicated with black arrowheads.